Title page

Effect of Dynamic Stiffness of Fasteners on Vibration and Acoustic Radiation of a ballastless Track

Han-Wen Xu, born in 1993, is currently a PhD candidate at *State Key Laboratory of Traction Power*, *Southwest Jiaotong University, China*.. He received his Master degree from *Dalian Jiaotong University, China*, in 2019. His research interests include high speed Wheel/rail noise and vibration and Vehicle-track coupling dynamics.
Tel: 13550116281; E-mail: xuhanwen@my.swjtu.edu.cn

Jian Han, born in 1987, is currently a postdoctoral research fellow at *Southwest Jiaotong University, China*. He received his PHD degree on from *Southwestern Jiaotong University, China*, in 2018.
E-mail: super_han@126.com

Xin-Biao Xiao, is currently a associate researcher and a PhD candidate supervisor at *State Key Laboratory of Traction Power, Southwest Jiaotong University, China*. His research interests include railway vehicle system dynamics and noise of high-speed train, vehicle/track coupling dynamics and derailment.
E-mail: xinbiaoxiao@163.com

Xiao-Long Liu, is currently a PhD candidate at *State Key Laboratory of Traction Power, Southwest Jiaotong University, China.*
E-mail: lxl@my.swjtu.edu.cn

Mou-Kai Liu, is currently a PhD candidate at *State Key Laboratory of Traction Power, Southwest Jiaotong University, China*.
E-mail: 993955719@qq.com

Xue-Song Jin, born in 1956, is currently a professor and a PhD candidate supervisor at *State Key Laboratory of Traction Power, Southwest Jiaotong University, China*. His research interests include wheel-rail interaction, rolling contact mechanics, railway vehicle system dynamics and noise of high-speed train.
E-mail: xsjin@swjtu.edu.cn

Corresponding author：Prof. Xue-song Jin　E-mail：xsjin@swjtu.edu.cn

Effect of Dynamic Stiffness of Fasteners on Vibration and Acoustic Radiation of a ballastless Track

Han-Wen Xu[1] • Jian Han [2] • Xin-Biao Xiao[1]• Xiao-Long Liu[1] • Mou-Kai Liu[1] • Xue-Song Jin[1*]

Received June xx, 201x; revised February xx, 201x; accepted March xx, 201x

Abstract: A new model for a single wheel rolling over a metro ballastless track is developed. It is used to carry out the analysis on the effect of dynamic characteristics of fastener on the vibration and noise radiation of the wheel and the track in the vertical direction, under the excitation of the wheel/rail uneven surfaces in detail. In this analysis, a rail is modeled as a Timoshenko beam resting on discrete rubber booted short sleepers, and the sleepers are connected with the slab through linear springs and damping units, the slab is modeled by using the FE method, the fastener is characterized by using the Poynting-Thomson model which takes into account that the stiffness and dumping of the fasteners vary with vibration frequency in their service. The dynamic characteristics of the fastener include the variation of its stiffness and damping with frequency. The analysis considers that the fastener dynamic stiffness increases with the excitation frequency while its damping decreases. The vibration and acoustic radiation of the wheel/track is, to varying degree, affected by the dynamic property of the fastener. The vibration and acoustic radiation of the sleeper and the slab is greatly affected by the dynamic property of the fastener. But the effect of the total noise level of the wheel and the track by the dynamic property of the fastener is not so large because the wheel and rail noise is dominant in the whole analyzed system. These conclusions have certain reference values for the study of the vibration and noise reduction measures of the wheel and track coupled system using the fastening characteristic.

Key words: Fastener • Dynamic stiffness • Wheel/rail rolling noise • P-T model • Rubber booted short sleeper track

✉ Xue-song Jin
xsjin@swjtu.edu.cnm

[1] State Key Laboratory of Traction Power, Southwest Jiaotong University, Chengdu 200240, China
[2] School of Mechanical Engineering, Southwest Jiaotong University, Chengdu 200240, China

1 Introduction

The rapid development of China's railways has changed the travel efficiency of its citizens[1]. With train speed increase, wheel/rail interaction becomes fiercer. This leads to the increase of vibration and sound radiation in wheel-rail rolling contact. To address this drawback a variety of vibration damping tracks were bred, and rubber booted short sleeper track is one of them. Compared to the slab track, the vibration damping tracks can improve track vibration isolation performance. Many researches were published on the vibration reduction of the rubber booted sleeper track, and its vibration reduction effects were found through the field tests and theoretical analysis[2,3]. But the good vibration isolation capability results in intense wheel-rail interaction, which leads to fatigue failure of key components of train and track[4], rail corrugation generation[5] and high-level wheel/rail noise. So a deep study regarding this problem is necessary.

Nowadays in the models of rubber booted sleeper track, almost no consideration was given to the effect of fastener dynamic stiffness on the dynamical behavior of the track. In fact, the rail pad inserting in the fastener is made of rubber. The stiffness and damping of it could be affected by the external excitation frequency, environmental temperature and preload, and in turn influence the vibration and noise radiation of the track.

Laboratory measurements of the fastener dynamic stiffness were described in Refs. [6,7]. In the measurements the vertical and lateral dynamic stiffness of the rail fastener systems have been measured using an indirect-method. The test results show that in the high frequency range (0-1 000 Hz) the stiffness and loss

factor change significantly with the excitation frequency change. A. Fenander analyzed the effect of the external excitation frequency and preload on the rail pad stiffness both in the tests of laboratory and operation lines[8]. The results indicate that the preload has a greater impact on the rail pad stiffness, compared to the external excitation frequency. A fraction derivate model was used to represent the dynamic characteristics of the rail pad. Later J. Maes present an method for rail pad testing, allowing for the measurement of stiffness and damping values between 20 and 2 500Hz under variable preload[9], then the characteristics of the stiffness and damping of the elastic pad changing with the external excitation frequency and preload were simulated by using the improved Poynting-Thomson mechanical model (the P-T model). In order to find out the dynamic characteristics of elastic pad under external higher frequency excitation, the time-temperature superposition method was applied, and the generalized Maxwell model was used to capture the dynamic stiffness damping mechanism of the elastic pad. It was found that the numerical results fit well with the field test data[10]. From the above research, it can be concluded that with the increase of the external excitation frequency, the stiffness and damping of the fastener change greatly.

In order to have a better understanding of the effect of the fastener dynamic properties on vehicle/track dynamic performance, various fastener models were proposed. Wei used the logarithmic fitting function to characterize the stiffness and damping frequency-dependent characteristics of the fastener, and used this model to analyze the vibration characteristics of the track and the vehicle/track coupling system, and their impact on the subway tunnel environment vibration[11-13]. At the same time, the temperature characteristic of the fastener stiffness was studied and its influence on the random frequency response characteristics of wheel/rail interaction was analyzed. Then the wheel/rail vibration and noise in frequency domain were derived, which accounts for the characteristics of frequency-dependent stiffness of rail fastener by adopting the logarithmic fitting function[14]. In the time domain a nonlinear fractional derivative viscoelastic model was used to analyze the influence of frequency-dependent and amplitude-dependent properties of the fastener on the dynamic characteristics of vehicle-track coupling system[15].

So far, the analysis of the dynamic stiffness characteristics of the fastener has mainly been conducted in low frequency domain. It is rarely mentioned in published papers regarding the analysis of the stiffness and damping frequency-dependent characteristics of fasteners influencing on the vibration and noise of the wheel rolling on the rubber booted short sleeper track. In this paper, a new model for a single wheel rolling over a metro ballastless track is developed in order to find out the high frequency vibration and noise characteristics of the wheel and the track parts with considering the influence of the dynamic stiffness and damping of the fasteners. The P-T mechanical model is used to represent the frequency-dependent characteristics of damping and stiffness of rail fastener, and the model is validated through the experimental test data.

2 Wheel/rail interaction model

The wheel/track interaction model used in predicting the vibration and sound radiation of the wheel/track is shown in Figure 1. This model considers that a single wheel rolls on a rubber booted short sleeper track, and their coupling is replaced with a contact spring. When the wheel moves along the rail the irregularity excitation between them is replaced with the 'moving' roughness, which means the roughness 'strip' is pulled through the gap between the wheel and the rail.

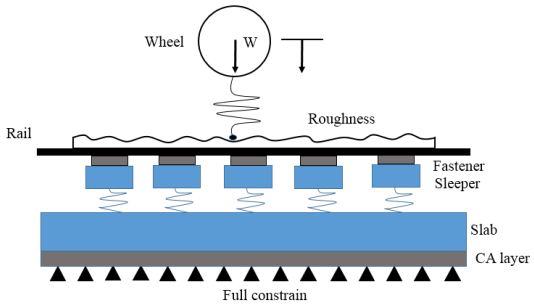

Figure 1 Wheel/track coupling system

2.1 Track model with frequency-dependent stiffness and damping of fasteners

2.1.1 *frequency-dependent fastener model*

The ordinary fastener models, Kelvin model (the K-V model) which can be seen in Figure 2 (a), considers frequency-independent stiffness and damping only. In this paper the P-T model is used to capture the frequency-dependent characteristics of the fastener. The P-T model is shown in Figure 2 (b).

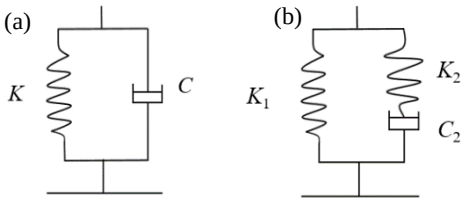

Figure 2 Fastener models, (a) Kelvin model, (b) P-T model

The parameters of the P-T model are shown in table 1. K_1 is the frequency-independent stiffness; K_2 is the frequency-dependent stiffness; C_2 is the frequency-dependent viscous damping, the coefficient $\alpha = \omega^2/(\omega^2+z)$ and $z=K_t/C_t$, ω is the radian frequency.

Figure 3 shows the comparison of the fastener dynamic stiffness results of the P-T model and the laboratory measurement data. In the figure three different fastener stiffness data were used to verify the P-T model[6, 7], and their static stiffness are , respectively, 6 kN/mm, 75 kN/mm and 280 kN/mm.

Table 1 P-T model parameters

Property	P–T model
K_t	$K_1+K_2 \cdot 2\alpha$
C_t	$C_2\alpha\frac{z^2}{\omega^2}$

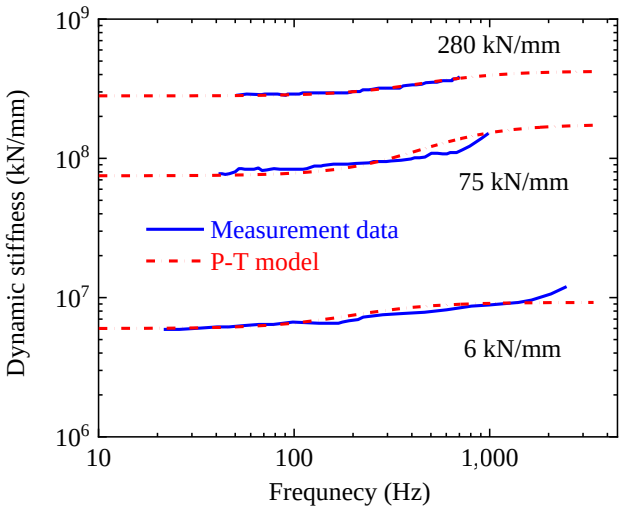

Figure 3 Dynamic stiffness of the P-T model

It is difficult to accurately obtain the dynamic damping value of the fastener in a laboratory. The stiffness K_t and damping C_t of the P-T modal are proportionable, which means if the dynamic stiffness is approximately consistent with the experimental results, the damping matches the field measurement data in the range of the error permitted. As it can be seen in Figure 4 the frequency-dependent characteristic of the damping and stiffness of the fastener can be captured by using the P-T model in the frequency range of 0-2 000 Hz. It can be concluded that the P-T model has good applicability for characterizing the fastener of dynamic stiffness and damping, and can reflect the vertical frequency-dependent variation characteristics of the stiffness and damping of the fastener.

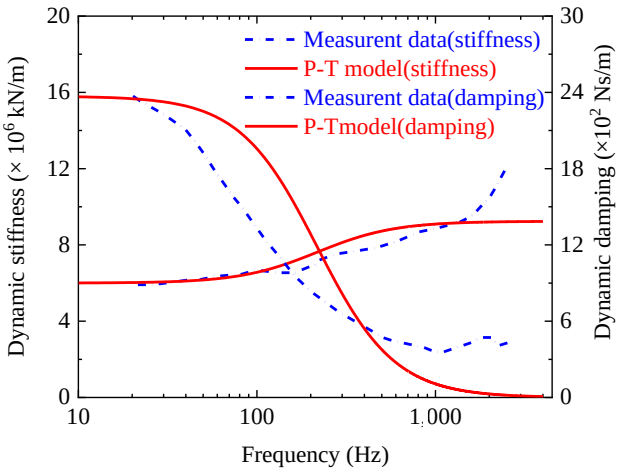

Figure 4 Dynamic stiffness and damping of the P-T model

2.1.2 *Track model of rubber booted short sleeper*

For the model of rubber booted short sleeper track, the rail is simulated by using the Timoshenko beam, the rubber booted short sleeper is simplified as a mass block, and the rubber support under the sleeper is simulated by using a linear damping-spring, and the slab is modeled with the FE method. The relevant parameters are shown in table 2.

Table 2 Track parameters

Parameters	Value
Rail density ρ_r	7850 kg/m^3
Rail cross-section area A_r	7.69×10^{-3} m^2
Rail Shear factor κ	0.4
Rail Shear modulus G_r	0.77×10^{11} Pa
Rail young's modulus E_r	2.1×10^{11} Pa
Sleeper pad stiffness k_s	30 kN/mm
Sleeper pad damping c_s	1×10^4 Ns/m
Sleeper mass M_{sn}	90 kg
Sleeper space	0.57 m

The track motion equation in frequency domain is denoted by Eqns. (1)~(4), Eq. (1) and Eq. (2) are the rail equations, Eq. (3) is the equation of the sleeper, and Eq. (4) is the slab equation. In these equations, N is the total number of the fasteners involved in the numerical simulation, N_p is the number of the fasteners on one slab, ω is the radian frequency, u_r is the rail receptance, u_{sn} is the sleeper receptance, u_{slab} is the slab receptance, and ϕ indicates the rotation of the cross-section relative to the un-deformed axis.

$$-\rho_r A_r \omega^2 u_r + G_r A_r \kappa(\phi' - u_r'') + \sum_{n=1}^{N} K_p (u_r - u_{sn}) \delta(z - z_{sn}) = F\delta(z) \quad (1)$$

$$-\rho_r I_r \omega^2 \phi + G_r (1 + i\eta_r) A\kappa(\phi - u_r') - E_r I_r (1 + i\eta_r) \kappa\phi'' = 0 \quad (2)$$

$$-\omega^2 M_{sn} u_{sn} + (u_{sn} - u_r(z_n)) \cdot K_p + (u_{sn} - u_{slab}(z_{ln})) \cdot K_s = 0 \quad (3)$$

$$-\omega^2 \rho_s A_s \omega^2 u_{slab} + E_s I_s u_{slab}'''' + K_b \cdot u_{slab} + \sum_{n=1}^{Np} K_s \cdot (u_{slab} - u_{sn}) \delta(z_l - z_{ln}) = 0 \quad (4)$$

In Eqns. (1)~(4), ρ, E and G with foot marks are, respectively, the density, the Yong's modulus, and shear modulus, the subscripts r and s means the rail and the slab, respectively. κ is the shear coefficient of the rail. K_s is the rubber structure between the sleeper and the slab, K_p=K_t–iωC_t is the total stiffness of the fastener (K_t and C_t are the frequency-dependent stiffness and damping of the fastener, respectively), K_s=k_s–iωc_s is the total stiffness of the elastic support between the sleeper and the slab (k_s and c_s are, respectively, the stiffness and damping of the elastic support between the sleepers and slab), and K_b =k_b(1+iη_b) is the total stiffness of the elastic support under the slab (k_b and η_b is, respectively, the stiffness and loss factor of the elastic support structure under the slab), the slab parameter in this paper can be found in Ref. [16].

The vertical frequency response function of the rail is indicated by Eq. (5).

$$u(z_j) = F\alpha(z_j, 0) - \sum_{n=1}^{N} F_{pn}\alpha(z_j, z_n), \quad j = 1, 2, ..., N \quad (5)$$

$$F_{pn} = K_p[u_r(z_{pn}) - u_{sn}] \quad (6)$$

In the Eq. (5), F_{pn} is the vertical force between rail and sleeper, which can be obtained by using Eq. (6), and $u_r(z_{pn})$ and u_{sn} is the receptances of the rail and the sleeper, respectively, at the fastener.

The vertical frequency response function of the slab is denoted by Eq. (7), and the force between the sleeper and slab is indicated by Eq. (8). z_{lm} is the position of F_{slm} imposed on the slab, l is the serial number of the slabs used in the calculation, m is the serial number of the fasteners imposed on the slab, and the slab displacement can be obtained by using Eq. (7)[16]:

$$u_{slab}(z_l) = \sum_{m=1}^{N_p} F_{slm}\beta(z_l, z_{lm}) \quad (7)$$

$$F_{slm} = K_s[u_{slab}(z_{lm}) - u_{sn}], \quad l = 1, 2, ..., N/10, \quad m = 1, 2, ...N_p \quad (8)$$

By means of the modal superposition method $\beta(z_l,z_{lm})$ in Eq. (7) can be obtained, as indicated by Eq. (9).

$$\beta(z_1, z_2) = \sum_{n=1}^{N_m} \frac{W_n(z_1) W_n(z_2)}{(1 + i\eta_{slab})\omega_n^2 - \omega^2 + (1 + i\eta_b)\omega_f^2} \quad (9)$$

In Eq. (9), $W_n(z)$ is the modal shape function of the plate with free edge, ω_n is the natural frequency of rectangular plates with free edges, ω_f is the natural frequency of the rectangular plate resting on the Winkler foundation with free edges, η_{slab} is the loss factor of the slab, and N_m is the number of the free rectangular plate modes.

The finite element model of the slab and its modal shapes are shown in Figure 5, the highest analysis frequency of the slab is 253 Hz which is proper for the analysis of the track vibration characteristics.

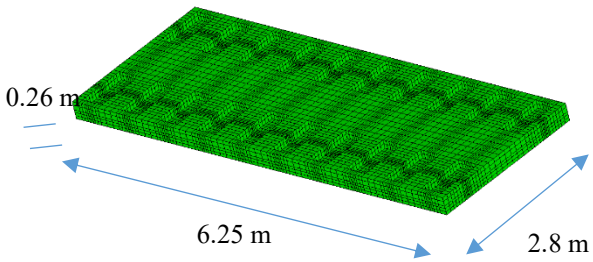

(a) Slab finite element model

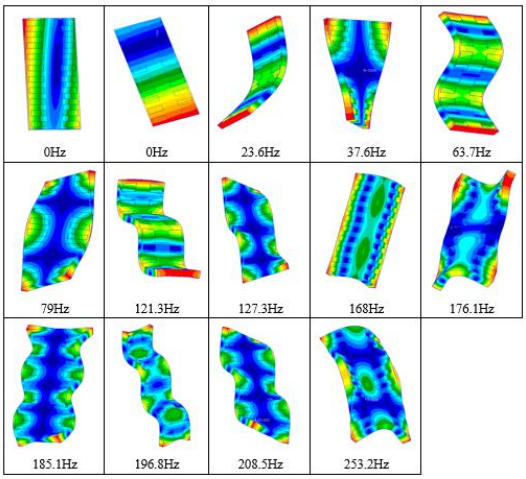

(b) Slab modal shapes

Figure 5 Slab finite element model and modal shapes

2.2 Model of the wheel

The wheel is modeled by using the finite element method, the wheel eigenmodes and natural frequencies are obtained. The finite element mesh of the wheel cross-section is shown in Figure 6.

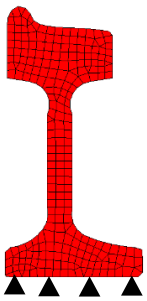

Figure 6 Wheel finite element model

Based on the modal superposition method the frequency response of the wheel can be predicted[5]. The wheel hub is fully constrained, and the unit force input at the wheel/rail contact point. Then the receptance of the wheel can be calculated by using Eq. (10).

$$\alpha_{jk}(\omega)=\sum_{r=1}^{N}\left(\frac{\varphi_{jr}\varphi_{kr}}{M_r\omega_r^2(1-\omega_{mr}^2+2\mathrm{i}\,\xi_r\omega_{mr})}\cdot\cos(n\alpha)\right) \tag{10}$$

In Eq. (10), r indicates the r^{th} modal, φ_{jr} and φ_{kr} are the rth modal shape functions at node x_j and x_k, respectively. M_r is defined as the modal mass, ω_r is the angular frequency of the wheel, and ω is the circular frequency. $\omega_{mr}=\omega/\omega_r$ is the frequency ratio, and ξ_r is the modal damping ratio which can be derived from measurement. The wheel radius R is 0.43m, its density is 7850 kg/m^3, poisson' ratio μ is 0.3, and young's modulus E is 2.1×10^{11} Pa.

2.3 Model of wheel/rail interaction

2.3.1 *Rail/wheel combined roughness*

In this paper the vertical vibration and acoustic radiation of the wheel and the track are analyzed only. According to the TWINS model, it can be known that the irregularities on the surfaces of wheel and rail can induce wheel/rail dynamic force which can be calculated by the surface roughness of the wheel and the rail (the roughness wavelength related to the vibration and noise of the wheel and the rail is mainly concentrated in the range of 5 mm to 500 mm). When analyzing the wheel/rail interaction, it is necessary to select appropriate roughness values of the wheel and the rail. The roughness spectra used in the calculation are the 'irregularity' spectra of rail (class C) and wheel (class C) surfaces, which were obtained through a large number of field test in the HARMONOISE project[17]. The roughness spectra are shown in Figure 7.

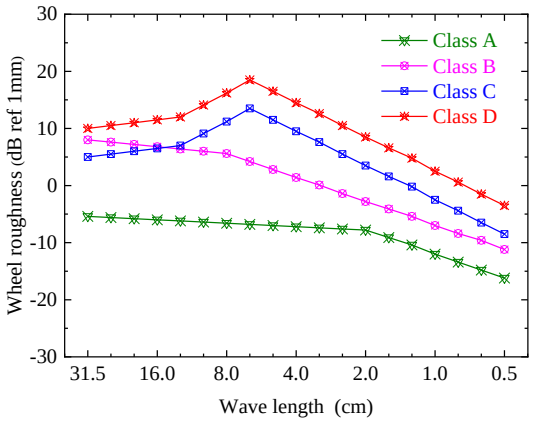

(a) Wheel roughness spectra

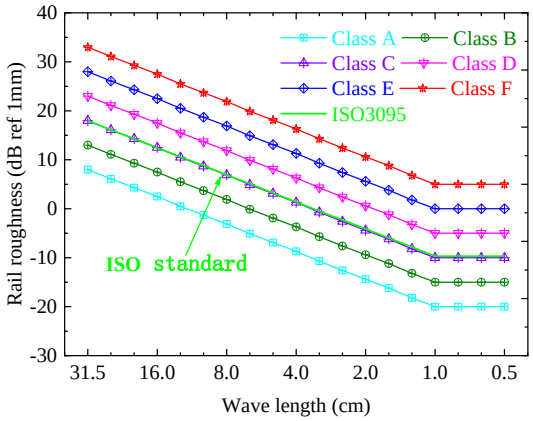

(b) Rail roughness spectra

Figure 7 Roughness spectra of wheel and rail[19]

2.3.2 *Contact filter*

The contact area between wheel and rail is an ellipse with half axis lengths of a and b. Then if the roughness wavelength of the rail and wheel surfaces in the longitudinal direction is shorter than or equal to 2a the effect of the roughness could be neglected through the filter function. The estimated filter function of the contact region is expressed with Eq. (11).

$$|H(k)|^2=\frac{4}{\alpha(kb)^2}\int_0^{\arctan\alpha}[J_1(kb\sec x)]^2\,dx \tag{11}$$

$J_1(x)$ is the first-order Bessel function, b is the contact circle radius, k is the roughness wave number, and α is the correlation coefficient of the wheel and rail

surface roughness.

The train speed considered in this paper is 60 km/h, the wheel radius is 0.43 m, and the rail is UIC60[6]. Based on Eq. (11) the combined roughness spectrum of the wheel and the rail is shown in Figure 8.

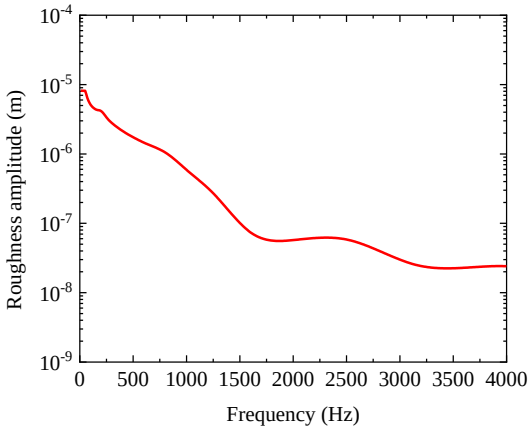

Figure 8 Combined roughness of wheel and rail

2.3.3 Contact stiffness

The vertical contact stiffness is indicated by Eq. (12).

$$k_{\mathrm{H}}=\frac{3}{2\zeta}\frac{4}{3}\cdot\left(\frac{E}{1-u^{2}}\right)^{2}P_{0}\frac{4R_{\mathrm{W}}R_{\mathrm{R}}}{R_{\mathrm{W}}+R_{\mathrm{R}}} \tag{12}$$

R_{w} is the wheel radius, R_{R} is the transverse railhead curvature radius, E is the young's modulus of the rail and the wheel, μ is the Poisson's ratio, P_0=60 kN is the static load of a single wheel, ξ is a dimensionless quantity dependent on the curvature radii of the two surfaces, the relation between ξ and θ can be seen in Ref [17]. θ is written as

$$\theta=acr\cos\left|\frac{R_{\mathrm{R}}-R_{\mathrm{W}}}{R_{\mathrm{R}}+R_{\mathrm{W}}}\right| \tag{13}$$

Then the contact stiffness can be calculated and it reads as k_{H}=1197 kN/mm. The vertical dynamic force between the wheel and the rail can be calculated by using

$$F=-\frac{R}{\alpha^{\mathrm{W}}+\alpha^{\mathrm{R}}+\alpha^{\mathrm{C}}} \tag{14}$$

In Eq. (14), R is the combined roughness spectrum, α^{W} is the flexibility of the wheel, α^{R} is the rail flexibility, α^{C} is the contact stiffness flexibility, and $\alpha^{\mathrm{C}}=1/k_{\mathrm{H}}=8.36\times10^{-10}$ m/N.

2.4 Wheel/rail sound radiation model

The sound power of the rail and the sleeper can be calculated by using Eq. (15)[17]

$$W_{\mathrm{r}}=\rho_{\mathrm{r}}c_{\mathrm{r}}Lh\left\langle V^{2}\right\rangle\sigma \tag{15}$$

where, ρ_{r} is the air density, c_{r} is the velocity of sound travel in the air, L=6.25 m is the length of the track used for calculation, h is the total projected length of the rail section contour in the horizontal direction, h=0.22 m, $<V^2>$ is the mean square value of time and space of the normal velocity of the rail surface vibration, it can be calculated by using

$$\left\langle V^{2}\right\rangle=\frac{1}{L}\int\left|V\right|^{2}dz \tag{16}$$

For the sleeper the sound radiation surface area is $L\times h$=0.32×0.7 m^2. The radiation ratio σ, is determined by the size and shape of the vibrating structure.

Analytical methods can be used to obtain the radiation ratio σ, when the structure is not complex. But for the rail and the sleeper, the radiation ratio can be calculated by the boundary element method (BEM)[17,18]. Also by using the boundary element method, the wheel acoustic radiation model is established. The wheel sound power can be calculated by using the boundary element method and the wheel-track coupled model.

3 Analysis on influence of frequency-dependent characteristic of fastener

In this chapter the vibration and noise radiation of the wheel and the track parts is analyzed by using the P-T model and the K-V model. Compared with the slab track, the rubber booted short sleeper track can effectively reduce the vibration of the slab, but vibration is transmitted from the rail to the sleeper, which bring new structural vibration and noise radiation. So the further research is needed.

3.1 Mobility characteristic of track parts

Using the two models calculates the vertical rail mobility again the frequency increase, under unit impulse force excitation. They are shown in Figure 9. The frequency-dependent characteristic of stiffness and damping of the fastener has a great influence on the rail second-order bending vibration. The frequency of the rail second-order bending vibration modal increases from 250 Hz to 280 Hz, and the amplitude of the modal shape also increases. It is caused by the fastener stiffness increase and the damping decrease, rail corrugations are often found at this frequency band, therefore, attention should be paid to the vibration characteristics of the fastener. The rail modal shape of 3 020Hz is shown in Figure 10. It can be seen that at 3 020 Hz the rail vibration wave peak is at the fastener, so the decrease of the fastener damping can increase the rail vibration amplitude greatly.

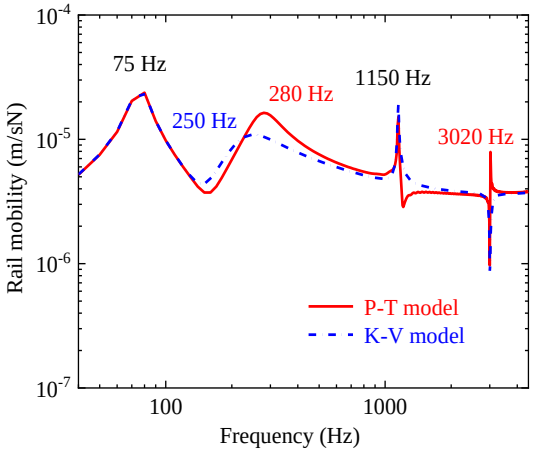

Figure 9 Rail vertical mobility

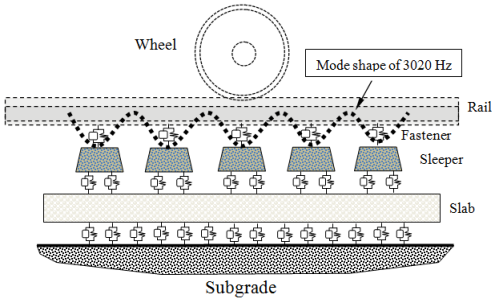

Figure 10 Rail vibration shape at 3020 Hz

Figure 11 shows the mobility of the sleeper. It can be observed that the ordinary fastener model underestimates the amplitude of the sleeper vibration at 190-630 Hz and overestimate above 630 Hz. In the lower frequency range, the rail vibration transmitted to the sleeper is mainly affected by the fastener stiffness, and the stiffer fastener can transmit more energy to the sleeper, while at higher frequencies the transmission is influenced by the damping, and the decrease of the fastener damping results in less energy transmission.

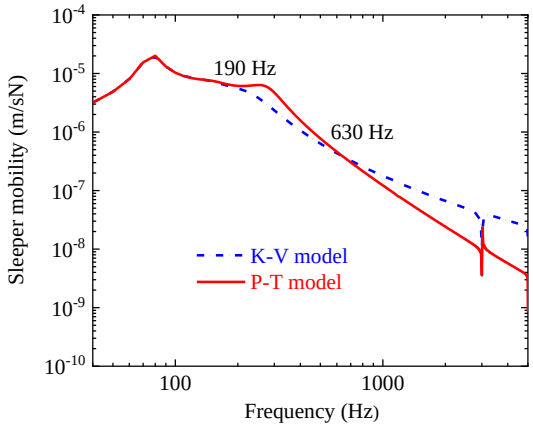

Figure 11 Vertical sleeper mobility

Figure 12 is the mobility of the slab. It can be seen that the dynamic effect of the fastener spreads to the slab. Their difference of the results obtained by using the two models can be observed from 100 Hz, and with the increase of the excitation frequency the slab mobility calculated with the P-T model is higher than that by using the K-V model in 240-1180 Hz range. Especially at 3020 Hz, its dynamic influence is similar to that on the sleeper.

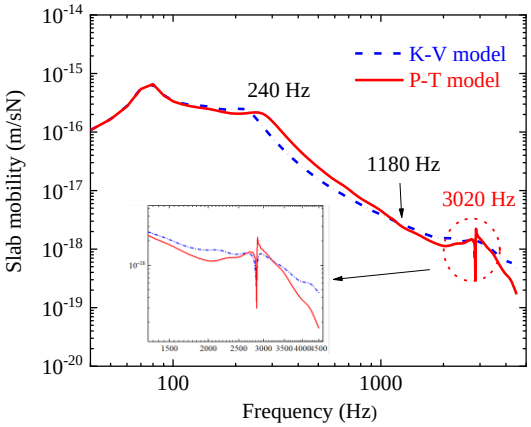

Figure 12 Vertical slab mobility

3.2 Vibration and acoustic radiation of wheel, track parts, correlation coupling parts

This section analyzes the effect of the dynamic stiffness and damping of the fastener on the vibration and noise of the wheel, the track parts, the correlation coupling parts, with considering the effect of wheel and rail surface roughness excitation. The roughness of Class C is used as the roughness excitation of the wheel and the rail in the analysis. In the calculation the train operation speed is 60km/h.

Firstly, by using the two models, the vertical vibration velocities of the rail, the sleeper and the slab are analyzed with considering the dynamic stiffness and damping of the fastener. Secondly, their acoustic radiation power is calculated in turn

The results of the rail are shown in Figure 13. The frequency-dependent characteristics of the fastener mainly affect the vertical rail velocity in the area around 3 020Hz. This is because the fastener damping is reduced in the frequency area, which means the lower constrain to the rail. Figure 13 indicates that the variation of stiffness and damping of the fastener with frequency effects on the rail vibration only in the higher frequency range under the wheel/rail roughness excitation.

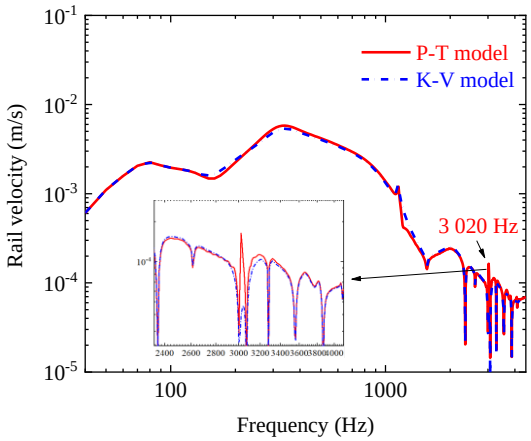

Figure 13 Rail velocity under wheel/rail roughness excitation

The sleeper vibration velocity under the wheel/rail (roughness excitation) force is shown in Figure 14. The difference between the results calculated with the two fastener models is obvious above 150 Hz. The vertical sleeper velocity calculated with the P-T model is higher than that with the K-V model in 150-630Hz range, which is caused by the fastener stiffness increase. At higher frequencies, the fastener damping decrease results in the low vibration energy transmitted from the rail to the sleeper, which also means that the K-V model could overestimate the vibration level of the sleeper at higher frequencies, as shown in Figure 14. But it could underestimate the sleeper vibration in the middle frequency range.

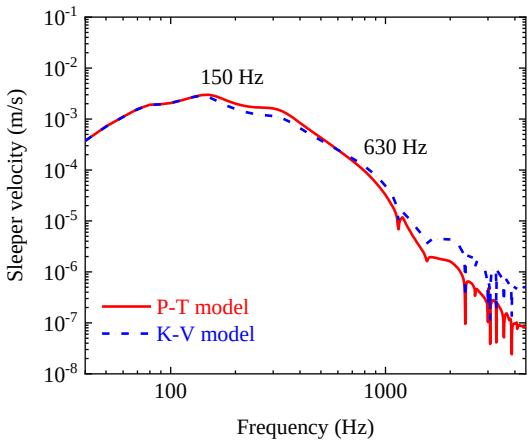

Figure 14 Sleeper velocity under wheel/rail roughness excitation

Compared to the Figure 14, the velocity of the slab in the Figure 15 has the similar phenomenon occurred in the middle frequency range. In the frequency range of 250-1 150 Hz, the slab velocity is higher than the result with the K-V model when considering the fastener dynamic effects. With the decrease of the damping, less energy transmitted from the rail to the sleeper results in lower slab vibration, in other word, the vibration isolation effect between the rail and the sleeper is overrated.

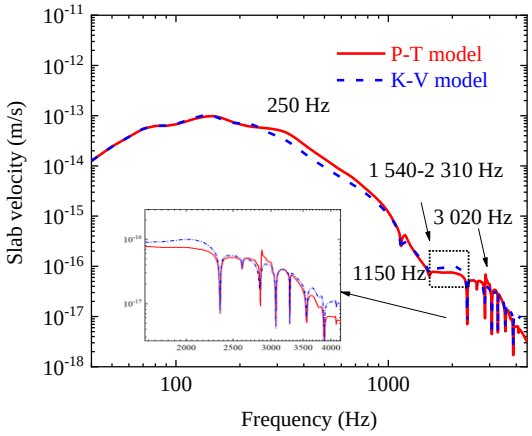

Figure 15 Slab velocity under wheel/rail roughness excitation

From Figures. 13~15, the conclusion can be drawn: the fluctuation features of the rail, sleeper and slab under wheel/rail roughness excitation are quite similar to the mobilities of the rail, sleeper and slab (without roughness excitation), respectively. The K-V fastener model could be used to carry out more reasonable and accurate calculations in track dynamical behavior.

The wheel vibration under the wheel/rail roughness excitation is studied. It is found that the vibration of the wheel is not sensitive to the change of the dynamic stiffness and damping of the fastener. This means that the change of the dynamic stiffness and damping of the fastener has little effect on the sound radiation of wheel. So，the relevant calculation results will be omitted.

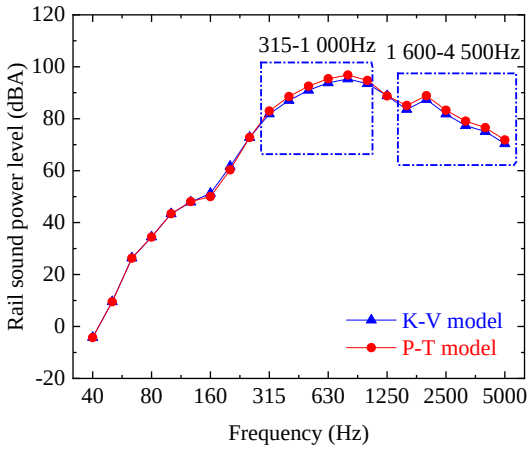

Figure 16 Rail sound power level under wheel/rail roughness excitation

The sound power of the rail under the wheel/rail roughness excitation is shown in Figure 16. The rail sound power calculated with the P-T model is higher than that obtained by using the K-V model in 315-4 500 Hz (except for 800 Hz). In this frequency band, the radiated sound power is about 1.2 dBA higher than that of the K-V model on average. Especially in the frequency band around 3 150 Hz, the rail sound power is about 1.7 dBA higher than that calculated with the K-V model. This is because the decrease of the fastener damping above 400 Hz results in a lower rail decay rate, which cause higher rail noise radiation power.

Figure 17 shows the sleeper sound radiation obtained by using the two models. It can be seen that the sleeper sound power obtained by using the P-T model is higher than that obtained by using the K-V model in 160-630 Hz. Their difference is about 2.2 dBA on average. But, using the K-V model could overestimate the sleeper sound radiation level in the frequency range of 1 000-4 500 Hz. The sleeper radiation sound power of the K-V model at 4 500 Hz frequency band is 24.7 dBA, which is 14.4 dBA higher than that of the P-T model. The vibration transmitting from the rail to the sleeper is increased by the fastener stiffness increase in the middle frequency range (160-630 Hz). At high frequencies the vibration transmission is influenced by the fastener damping, and the fastener damping decrease can result in a weak connection between the rail and the sleeper.

The slab vibration has a limited influence on the noise of the wheel/rail, and so the slab noise radiation is not considered in this analysis.

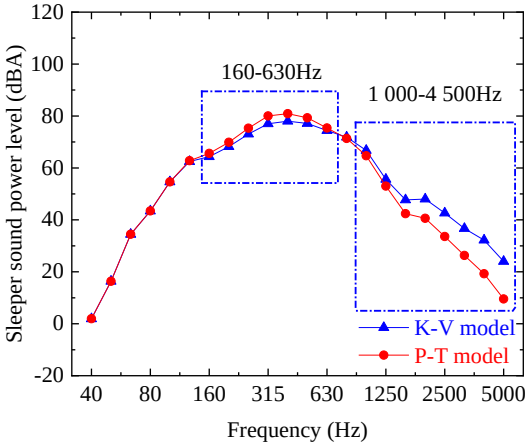

Figure 17 Sleeper sound power under wheel/rail roughness excitation

For the wheel/track combined rolling noise, it can be seen from Figure 18 that in the frequency of 160-2 500 Hz the wheel/rail rolling noise shows a higher level of the P-T model, compared to that of the K-V model. Their difference is about 1.5 dBA on average.

Figure 19 indicates the sound power levels of the related parts and the total wheel/track coupling system, and the difference of the results obtained by using the two models. In low frequency range, the wheel/track combined noise is mainly dominated by the sleeper, in the middle frequency range (250-1 600 Hz) the rail becomes the main source of the total wheel/track noise, while in high frequency range, the wheel is the major noise source. And the difference between the results of the two models is mainly in the frequency ranges of 160-1 000 Hz, 1 600-2 000 Hz, and above 4 500 Hz.

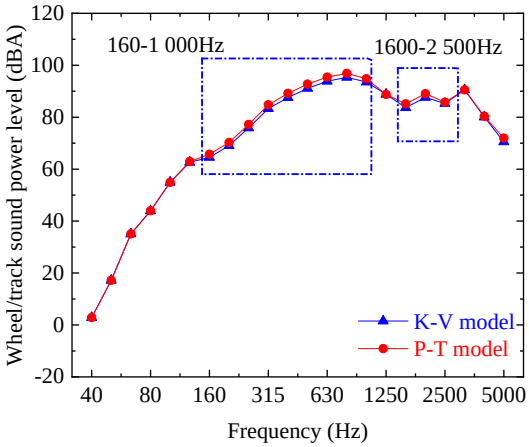

Figure 18 wheel/track sound power

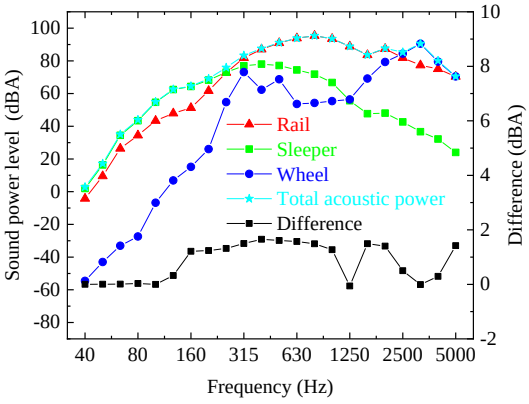

Figure 19 Radiated noise levels of the related parts and the total wheel/track coupling system, and noise difference between the results calculated with the two models

Table 3 shows the total radiation noise levels of the wheel/track under the combined roughness excitations of wheel/rail, which are calculated by using the two models. In the table, A-A indicates the combination of the wheel roughness A and the rail roughness A, B-B indicates the combination of the wheel's B and the rail's B, and so on. The surface roughness classification of the

wheel and the rail are shown in Figures. 6 and 7. When the combined wheel/rail surface roughness excitation drops from the A-A to the D-D, the total wheel/track sound power level increases from 109.7 dBA to 118.3 dBA. The average level of difference of the numerical results obtained by the two fastener model is from 0.6 dBA to 0.7 dBA. In this case, the impact of the dynamic stiffness and damping of the fastener is not so large on the total noise level of the wheel/track coupling system. This is because that although the dynamic stiffness and damping of the fastener has an big influence on the vibration and radiated noise of the sleeper and the slab the total noise of them is not dominant in the total noise of the wheel/track coupling system.

Table 3 Wheel/track radiation noise under different wheel/rail roughness excitation (without rail corrugation)

	A-A (dBA)	B-B (dBA)	C-C (dBA)	D-D (dBA)
P-T	109.7	112.6	115.5	118.3
K-V	109.1	111.9	114.8	117.6
Average Difference	0.6	0.7	0.7	0.6

3.4 Effect of rail corrugation on wheel/track noise radiation

Surface irregularities of rail and wheel give rise to the noise, ground-borne vibration, more additional dynamic loading and fierce wheel/rail interaction which leads to the larger noise radiation and causes the damage on the parts of the vehicle and the track [19-25]. In this chapter, the radiation noise analysis uses the 3 classical roughness of rail and wheel used in the HARMONOISE project and the rail corrugation roughness spectrum measured from a rubber booted short sleeper track in China subway line, as shown in Figure 20. The train speed is 60km/h

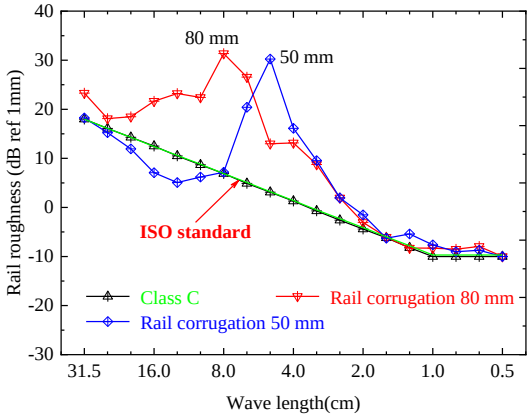

Figure 20 Spectra of rail corrugations and Class C roughness

With the increase of the track operation time, the interaction between the wheel/rail will cause rail corrugation, especially in the sharp curved track. Rail corrugation will lead to severe wheel-rail interaction. Rail corrugation wavelength depends on train operation speed and structural characteristics of track. So in this paper the field measured corrugation data of the rubber booted sleeper track (operating speed of 60 km/h) is used to analyze the wheel/rail rolling noise, combined with considering the effect of the wheel surface roughness of different classifications. The corrugation with wavelengths of 50 mm and 80 mm, shown in Figure21 and 22, is used in the analysis. For the operation speed of 60km/h and the corrugation of wavelengths of 50 mm and 80 mm, the corresponding corrugation passing frequencies are, respectively, 333.3Hz and 208.3 Hz.

Figures.21 and 22 indicate the sound power levels under the excitations of rail corrugation of wavelengths of 80 mm and 50 mm, respectively. (a), (b), (c) and (d) of the Figures denote the numerical results, with considering the excitations of the wheel roughness levels of A, B, C, and D, respectively. As can be seen in Figure 21 and Figure 22, when the corrugation occurs on the rail it will definitely and significantly increase the noise levels of the wheel/track and the related parts. For the corrugation excitation of 80 mm and 50 mm wavelengths, the sound power levels reaches their maxima at about the corrugation passing frequencies, 208.3 Hz and 333.3 Hz, respectively. But, for the corrugation excitation of the two different wavelengths, the noise level of the wheel is less than those of the rail and the sleeper at the frequencies less than about 1300 Hz. This is an open problem.

Due to the existence of the rail corrugation, the contribution of the rail noise to the total noise in the discussed full frequency domain is dominant for any wheel surface roughness. Above 2500Hz, the contribution of the wheel noise will dominate like the rail. Compared to the results of the rail corrugation excitation of 80 mm wavelength, as shown in Figure21, under the corrugation excitation of 50 mm wavelength, the noise levels increase more sharply in approaching the corrugation passing frequency of 333.3 Hz, as shown in Figure22. The maximum difference of the noise levels calculated with the two fastener models is close to 2 dBA, and the average level of the difference is 0.6-0.8 dBA, with considering the combined excitation of the rail corrugation with different wavelength and the different wheel surface roughness.

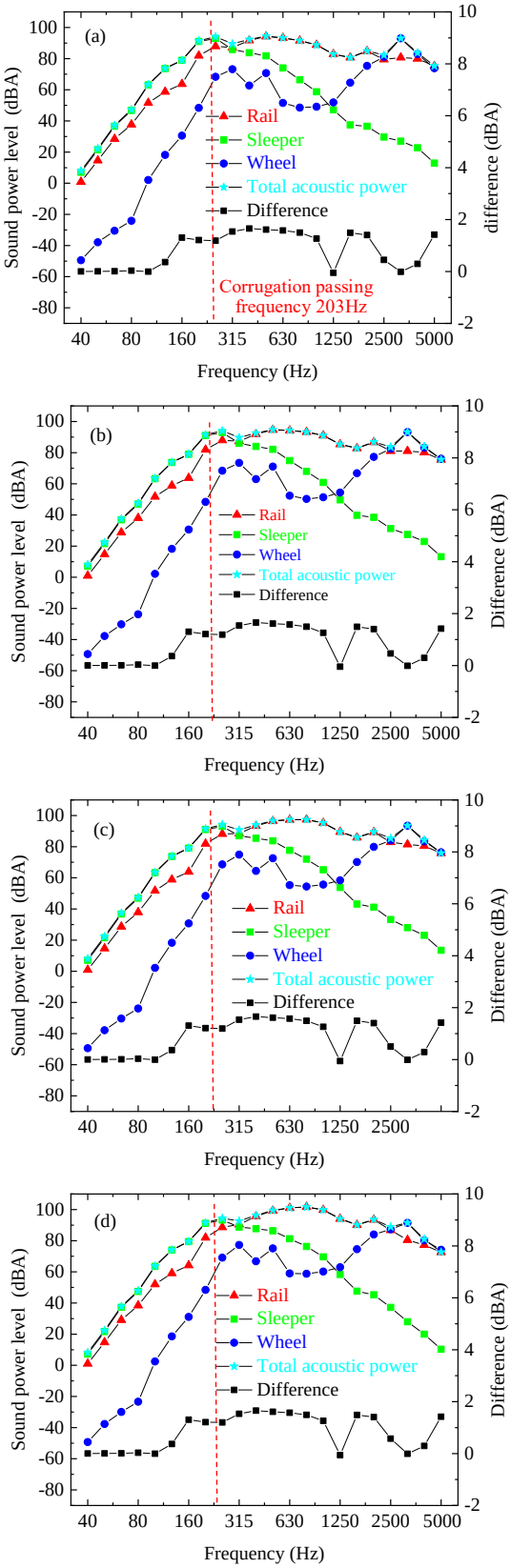

Figure 21 Sound power levels under rail corrugation excitation of 80 mm wavelength, with the combined examinations of (a) wheel roughness A, (b) wheel roughness B, (c) wheel roughness C, and (d) wheel roughness D

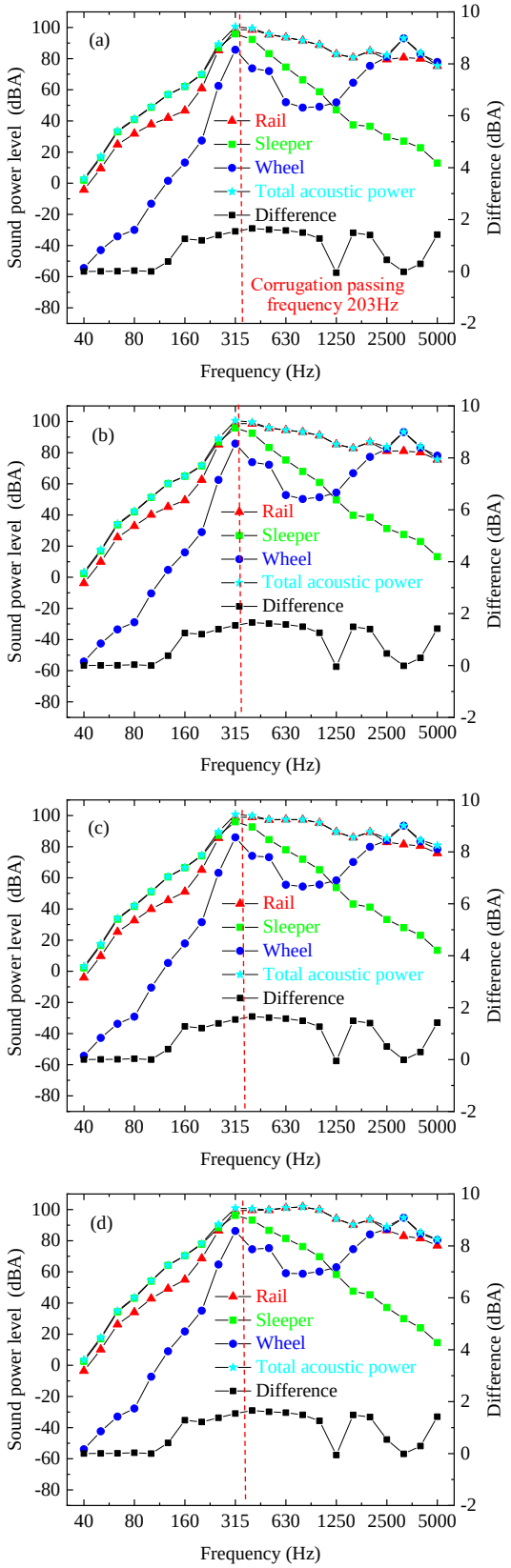

Figure 22 Sound power levels under rail corrugation excitation of 50 mm wavelength, with the combined examinations of (a) wheel roughness A, (b) wheel roughness B, (c) wheel roughness C, and (d) wheel roughness D

4 Conclusion

This paper presents the study on the effect of the dynamic stiffness of the fastener system on the vibration and acoustic radiation of a single wheel running on a rubber booted short sleeper track. In the study, the P-T model is used to improve the prediction accuracy of vibration and noise of the wheel coupled with the track. The influence of the fastener frequency-dependent characteristics is considered in the model, which is used to in detail analyze the vibration and acoustic of the wheel rolling on the rubber booted short sleeper track, with considering the combined excitation of the rail corrugation with different wavelength and different surface roughness of the wheel/rail. The conclusion can be drawn as:

1. In the analyzed frequency range of 5000 Hz, the change of the dynamic stiffness and damping of the fastener has the greatest influence on the resonance frequencies and amplitudes of the modal shapes of the rail, the influence on the sleeper is second, and the influence on the short sleeper is least. Special attention is required for the two bending resonant frequencies of the rail affected, 250 Hz and 1150 Hz (Rail Pined-pined resonant frequency), which are often the sources of rail corrugation[26,27].
2. The vibration and sound radiation level of the wheel coupled with the track is influenced to varying degrees by the dynamic stiffness and damping of the fastener system under the excitation of the wheel/rail irregularity (including rail corrugation). The influence range of the rail vibration velocity is above 2000 Hz, the influence range of the sleeper and the slab is above 200 Hz. The influence on the noise level of the sleeper is greatest (due to the change of energy transfer characteristics of the fastener), the influence on the rail noise is second, and the influence on the track is least. The maximum influence on the total noise level of the wheel/track is close to 2 dBA, and the average level is 0.6-0.8 dBA.
3. Due to the existence of the rail corrugation excitation, the contribution of the rail noise to the total noise of the wheel coupled the track, in the discussed full frequency domain, is dominant, compared to the excitation of any standard wheel surface roughness. Above 2500Hz, the contribution of the wheel noise will dominate like the rail. For the corrugation excitation, the sound power levels of all the discussed parts reaches their maxima at about the corrugation passing frequencies, and the higher the corrugation passing frequency (the shorter the wavelength of the corrugation), the faster the sound power level of the relevant analyzed parts increases in approaching the passing frequency.

7 Declaration

Acknowledgements

The authors sincerely thanks to Professor Bing-zhi Chen, of Dalian Jiaotong University for his critical discussion manuscript preparation.

Funding

The present work is supported by the National Natural Science Foundation of China (No. 52002340), the National Natural Science Foundation of China (No. U1934203), Science and Technology Research and Development Program of China Railway (N2019G037), Sichuan Science and Technology Program (2020YJ0076).

Availability of data and materials

The datasets supporting the conclusions of this article are included within the article.

Authors' Contributions

XH, JH, XL, and ML analyzed the data; H Xu wrote the paper; All authors read and approved the final manuscript.

Competing interests

The authors declare no competing financial interests.

Consent for publication

Not applicable

Ethics approval and consent to participate

Not applicable

REFERENCES

[1] X S Jin. Mechanics in performance of wheel-rail. *Journal of Mechanical Strength*, 2005, 27 (4): 408-418.

[2] X P Cai, D C Li, Y R Zhang, et al. Experimental Study on the Vibration Control Effect of Long Elastic Sleeper Track in Subways. *Shock and Vibration*, 2018, 13

[3] Z X He, X W Yang. Dynamic response analysis of an asymmetric coupled vehicle-track system generated by voided elastic two-block sleeper. *Shock and Vibration*, 2016.

[4] C Zhou, M R Chi, Z F Wen, et al. An investigation of abnormal vibration induced coil spring failure in metro vehicles. *Engineering Failure Analysis*, 2020, 108.

[5] X L Cui, G X Chen, J W Zhao, et al. Field investigation and numerical study of the rail corrugation caused by frictional self-excited vibration. *Wear*, 2017 (376-377) 1919-1929.

[6] D J Thompson, N Vincent. Track dynamic behaviour at high frequencies. Part 1: Theoretical models and laboratory measurements. *Vehicle system dynamics supplement*, 1995, 24: 86-99.

[7] D J Thompson. Development of the indirect method for measuring the high frequency dynamic stiffness of resilient elements. *Journal of Sound and Vibration*, 1998, 213(1), 169-188.

[8] A Fenander. Frequency dependent stiffness and damping of railpads. Proceedings of the Institution of Mechanical Engineers, *Part F: Journal of Rail and Rapid Transit*, 211(1), 51-62.

[9] J Maes. Measurements of the dynamic railpad properties [J]. *Journal of Sound and Vibration*, 2006 293: 557-565.

[10] M Oregui, A de Man. Obtaining railpad properties via dynamic mechanical analysis. *Journal of Sound and Vibration*, 2016 363: 460-472.

[11] K Wei. Effect of Frequency-Dependent Damping of Rail Pad on Environment Vibration of Subway Tunnel. *China Railway Science*, 2015, 36 (3): 17-23 (in Chinese).

[12] K Wei. Zhang P. Study on vertical natural vibrations of steel rail considering frequency-dependent stiffness of rail pads. *Journal of the China Railway Society*, 2016, 38 (6): 79-85 (in Chinese).

[13] K Wei, Zhang P. The Influence of Amplitude- and Frequency-Dependent Stiffness of Rail Pads on the Random Vibration of a Vehicle-Track Coupled System. *Shock and Vibration*, 2016.

[14] Q Yin, C B Cai, S Y Zhu. Effect of the frequency-dependent stiffness of rail fasteners on the wheel-rail vibration noise. *Journal of Vibration and Shock*, 2017, 26 (18): 408-418. (in Chinese)

[15] S Y Zhu, C B Cai. A nonlinear and fractional derivative viscoelastic model for railpads in the dynamic analysis of coupled vehicle–slab track systems. *Journal of Sound and Vibration*, 335(2015): 304-320.

[16] H P Liu. A study on modeling, prediction and its control of wheel/rail rolling noises in high speed railway. Shanghai Jiaotong University, 2013.

[17] T W Wu. Boundary element acoustics. Southampton: WIT Press; 2005.

[18] D J Thompson. Railway Noise and Vibration. 2009: 6-10.

[19] X L Liu. Study on the Cause of Abnormal Noise in the Cab of a Metro Train. Southwest Jiaotong University, 2017 (in Chinese).

[20] S L Grassie. Rail corrugation: characteristics, causes, and treatments. *Rail and Rapid Transit*, 2009, 223:581-596.

[21] J Han, X B Xiao, Y Wu, et al. Effect of rail corrugation on metro interior noise and its control. *Applied Acoustics*, 2018, 130:63-70.

[22] J J Kalker, F Periard. Wheel-rail noise-impact, random, corrugation and tone noise. *Wear*, 1996; 191:184-7.

[23] L Ling, W Li, H X Shang, et al. Experimental and numerical investigation of the effect of rail corrugation on the behaviour of rail fastenings. *Vehicle System Dynamic*, 2014; 52:1211-31.

[25] M VISCARDI, P NAPOLITANO. Wheel-Rail Interaction Based on Roughness Calculation. *WSEAS Transactions on Applied and Theoretical Mechanics*, 2017; 12 173-180

[26] XS Jin, W Li, Z F Wen, et al. An Investigation into Rail Corrugation, its Mechanisms and Effects on the Dynamic Behavior of Metro Trains and Tracks in China. *International Journal of Railway Technology*, 2016, 5(3):1-29.

[27] W Li. Study on root cause of metro rail corrugation and it's influence on behavior of vehicle-track system. Southwest Jiaotong University, 2010 (in Chinese).